crystals

MDPI

Article

3D-FEM Simulation of Hot Rolling Process and Characterization of the Resultant Microstructure of a Light-Weight Mn Steel

Ana Claudia González-Castillo [1], José de Jesús Cruz-Rivera [1], Mitsuo Osvaldo Ramos-Azpeitia [2], Pedro Garnica-González [3], Carlos Gamaliel Garay-Reyes [4], José Sergio Pacheco-Cedeño [5] and José Luis Hernández-Rivera [6,*]

1 Instituto de Metalurgia, Universidad Autónoma de San Luis Potosí, Sierra Leona 550, Lomas 2a Sección, San Luis Potosí C.P. 78210, Mexico; acg488@gmail.com (A.C.G.-C.); jdjcr35@uaslp.mx (J.d.J.C.-R.)
2 Facultad de Ingeniería, Universidad Autónoma de San Luis Potosí, Dr. Manuel Nava 8, Zona Universitaria, San Luis Potosí C.P. 78290, Mexico; mitsuo.ramos@uaslp.mx
3 División de Estudios de Posgrado, Tecnológico Nacional de México Campus Instituto Tecnológico de Morelia, Av. Tecnológico 1500, Michoacán C.P. 58120, Mexico; pedro.gg@morelia.tecnm.mx
4 Laboratorio Nacional de Nanotecnología, Centro de Investigación de Materiales Avanzados (CIMAV), Miguel de Cervantes 120, Chihuahua C.P. 31136, Mexico; carlos.garay@cimav.edu.mx
5 Escuela de Ingeniería y Ciencias Región Centro, Tecnológico de Monterrey Campus Morelia, Av. Montaña Monarca 1340, Michoacán C.P. 58350, Mexico; sergiopachecocedeno@gmail.com
6 CONACYT-Instituto de Metalurgia, Universidad Autónoma de San Luis Potosí, Sierra Leona 550, Lomas 2a Sección, San Luis Potosí C.P. 78210, Mexico
* Correspondence: luis.rivera@uaslp.mx

check for updates

Citation: González-Castillo, A.C.; Cruz-Rivera, J.d.J.; Ramos-Azpeitia, M.O.; Garnica-González, P.; Garay-Reyes, C.G.; Pacheco-Cedeño, J.S.; Hernández-Rivera, J.L. 3D-FEM Simulation of Hot Rolling Process and Characterization of the Resultant Microstructure of a Light-Weight Mn Steel. *Crystals* **2021**, *11*, 569. https://doi.org/10.3390/cryst11050569

Academic Editors: Grzegorz Golański, Hanna Purzyńska and Paweł Wieczorek

Received: 17 April 2021
Accepted: 17 May 2021
Published: 20 May 2021

Abstract: Computational simulation has become more important in the design of thermomechanical processing since it allows the optimization of associated parameters such as temperature, stresses, strains and phase transformations. This work presents the results of the three-dimensional Finite Element Method (FEM) simulation of the hot rolling process of a medium Mn steel using DEFORM-3D software. Temperature and effective strain distribution in the surface and center of the sheet were analyzed for different rolling passes; also the change in damage factor was evaluated. According to the hot rolling simulation results, experimental hot rolling parameters were established in order to obtain the desired microstructure avoiding the presence of ferrite precipitation during the process. The microstructural characterization of the hot rolled steel was carried out using optical microscopy (OM), scanning electron microscopy (SEM) and X-ray diffraction (XRD). It was found that the phases present in the steel after hot rolling are austenite and α'-martensite. Additionally, to understand the mechanical behavior, tensile tests were performed and concluded that this new steel can be catalogued in the third automotive generation.

Keywords: hot rolling; FEM simulation; medium Mn steel

1. Introduction

Recently, the automotive industry is focused on using materials that reduce the weight of vehicles, increase the resistance to impact and at the same time decrease the consumption of gasoline and the emission of gases [1,2]. Among the materials that can provide these characteristics, due to their good combination of high strength, ductility and formability, are the Advanced High Strength Steels (AHSSs) [3,4].

Nowadays the rolling process of the AHSSs is gaining importance due to their extensive use in the automotive industry [5]. Depending on the temperature used in the rolling process, it can be classified into: hot, warm and cold rolling. The hot rolling process carried out at a high temperature (austenitic region) makes it possible to reduce the flow stress and the strain hardening, resulting in a decrease of the rolling load and stresses. The knowledge of the slab temperature during the rolling process and the rollers heat transfer of the rolling mill can provide information of the microstructure developed in the

sheet [6]; the mechanical properties can even be affected due to the temperature changes in the rolling process [7,8].

In addition to temperature, there are other process parameters, such as strain, strain rate, etc. that must be better understood since they represent an important role on the metallurgical changes that the steel could experience during the hot rolling process [9,10]. The final product of hot rolling can exhibit some mechanical defects, including edge cracking, alligatoring, central burst and surface defects. These defects require special consideration because they increase the production costs and cause serious damage in products [11]. In order to achieve the more stringent requirements from consumers, the rolling process must be well controlled, therefore a thorough knowledge of the process control parameters is required.

Nowadays, computer modeling is a powerful tool to simulate different thermomechanical processes, thus, it has been used to investigate the technological aspects of different processes in the steel industry, such as continuous casting, extrusion, forging, hot rolling, heat treatment, etc. [12]. Rolling of flat rolled products involves the coupling of a large number of physical phenomena such as the deformation of the workpiece together with its thermo-metallurgical evolution and the thermal evolution of the rollers together with their mechanical deformation [13]. For the analysis of these physical processes, it is possible to use Finite Element Method (FEM) which is one of the most accurate methods for analysis of the plastic deformation. DEFORM-3D is an FEM-based software to simulate elastoplastic deformation process under hot and cold conditions [14,15].

In the literature, there are some investigations about the hot rolling process using DEFORM-3D: Kumar et al. [16] studied the roll bite deformation during a plate rolling process of a microalloyed grade steel and they found that the predicted roll force agreed well with the measured values; Faini et al. [17] investigated the effects of the hot rolling main parameters (i.e., percentage of reduction, cooling time, etc.) on void closure index of 316L stainless steel. Nevertheless, in the case of AHSS, there are scarce publications related to roll forming process by FEM simulations, such as the study done by Li et al. [18] where the material and mechanical properties of a cold-rolled DP980 steel were investigated through thermal simulation experiments using ABAQUS software; or, the work realized by Wang et al. [19] in which the fracture behavior of a DP980 steel is studied during roll forming processes by ABAQUS software.

In this work, a commercial FEM code, DEFORM-3D v.11, was used to describe the behavior of a medium Mn steel, which belongs to the third generation of AHHS, during the hot rolling process. Temperature evolution, effective strain and damage factor were evaluated by computer simulation. To complement the study a microstructural characterization of the experimental steel was carried out.

2. Materials and Methods

2.1. Steel Production

The nominal composition of the studied steel is presented in Table 1. This composition was established according to thermodynamic calculations in order to predict the stable phases in this steel (using the TCFE9 database of the ThermoCalc® software v2018b), since this composition has not been previously studied in the literature. After verifying that the simulations predict the desirable phases in a medium Mn steel, the steel was cast under vacuum conditions using a permanent mold with the following dimensions, 75 × 75 × 200 mm, employing a 10 kg induction furnace CONSARC, using high purity raw materials. The nominal composition was confirmed by optical emission spectroscopy (OES). After that, the slab was sectioned into pieces of 75 × 75 × 30 mm which was used as the input geometry for the simulation and experimental hot rolling process.

Table 1. Nominal composition of medium Mn steel.

Element	C	Al	Si	Mn	Fe
Weight%	0.12	1.7	1.8	10.4	Balance

2.2. FEM Simulation of Hot Rolling

The study performed rigid-plastic finite element simulations using a commercial FEM code DEFORM-3D v11. The system configuration for the hot rolling simulation consists of two rollers, two guides and the workpiece. The hot rolling parameters considered in this study were summarized in Table 2.

Table 2. Parameters for DEFORM-3D® simulation of the hot rolling process.

Parameter	Value
Workpiece	
Initial length of slab	75 mm
Initial width of slab	75 mm
Initial height of slab	30 mm
Final height of slab	3 mm
Slab initial temperature	1000 °C
Room temperature	20 °C
Friction coefficient (μ)	0.7
Heat transfer coefficient	5000 $W/m^2 \cdot K$
Work-rollers	
Material	AISI H13
Roll radius	50.8 mm
Rolling speed	20 RPM
Roll temperature	500 °C
Rolling pass	
Reduction/pass	1 mm
Number of passes	27

To carry out the simulation the following points were considered:

- The plastic hot flow behavior, based on previous results of the medium Mn steel hot compression tests, was fed into the software.
- The material was reheated at 1000 °C after every 4 rolling passes.
- The workpiece was free of residual stresses and strains at the initial state and after each reheating cycle.
- The model of the workpiece material was plastic.
- The rollers were considered as rigid materials.

2.3. Experimental Characterization of the Hot Rolled Steel

The conditions under hot rolling process was carried out were a pre-heating of the rollers at 500 °C and an initial slab temperature of ~1000 °C. A speed of the rollers of 20 rpm and a thickness reduction of 1 mm per rolling pass were established according to the simulation results. As in the simulation procedure, the hot rolling process was performed over 27 rolling passes, every 4 rolling passes a reheating to 1000 °C was applied and the final thickness of the sheet was 3 mm.

Microstructural characterization was carried out by optical microscopy using an OLYMPUS GX51 microscope and by scanning electron microscopy using a JEOL JSM-6610LV microscope, operated with an acceleration voltage of 30 kV. The samples for optical and scanning electron microscopy were etched with Vilella's solution (consisting of 95 mL of ethanol, 5 mL of hydrochloric acid and 1 g of picric acid). X-ray diffraction was realized in a Bruker D8 Advance diffractometer with CuKα radiation (λ = 0.15418 nm). The scanning interval taken in this test was 40 to 110° with a scan speed of 0.02 s^{-1}. For the quantitative analysis, the MAUD software v2.92 (Luca Lutterotti, University of Trento, Italy) and the

International Center for Diffraction Data (ICDD) database were employed. On the other hand, for the mechanical properties of the hot rolled steel, Vickers microhardness testing was performed using a Shimadzu-HMVG21 machine; and the tensile tests were done in a 100 kN Shimadzu AG-I machine at room temperature.

3. Results and Discussion

3.1. FEM Simulations

3.1.1. Temperature Distribution

The importance of the proper rolling temperature selection lies in the fact that the rolling load is dependent on the flow stress of the material, determining the relative ease with which the material can be deformed without any cracking problems. In order to obtain a homogeneous structure, hot rolling must be done in the area of the austenite phase (γ), for this reason an initial temperature of the hot rolling process simulation of 1000 °C was selected and as can be seen in Figure 1, this temperature is in the austenite zone.

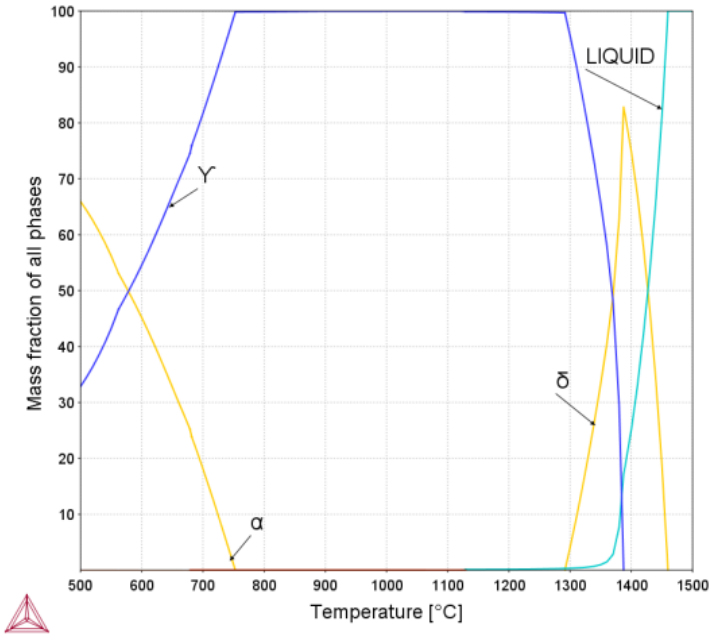

Figure 1. Distribution of phases as a function of temperature of the medium Mn steel.

In addition, it is important to predict the gradual decrease in temperature during rolling to select the number of rolling passes that can be applied in each cycle without ferrite formation occurring in the microstructure, so the temperature of the end of rolling has to be higher than Ar_3 temperature [20]. As can be seen in Figure 1, the Ar_3 temperature for this steel is 750 °C so the temperature at the end of rolling was selected to be close to 850 °C because this temperature is far enough from ferrite formation during the process.

The temperature distribution of rolling pass #1 (initial pass of 1st cycle), pass #4 (last pass of 1st cycle), pass #16 (last pass of 4th cycle) and pass #27 (last pass of 7th cycle), is presented in Figure 2a–d by an isometric cut of the slab. The final temperature at the center and surface of the sheet is presented in the Figure 2e, the evaluated points are shown in Figure 2a.

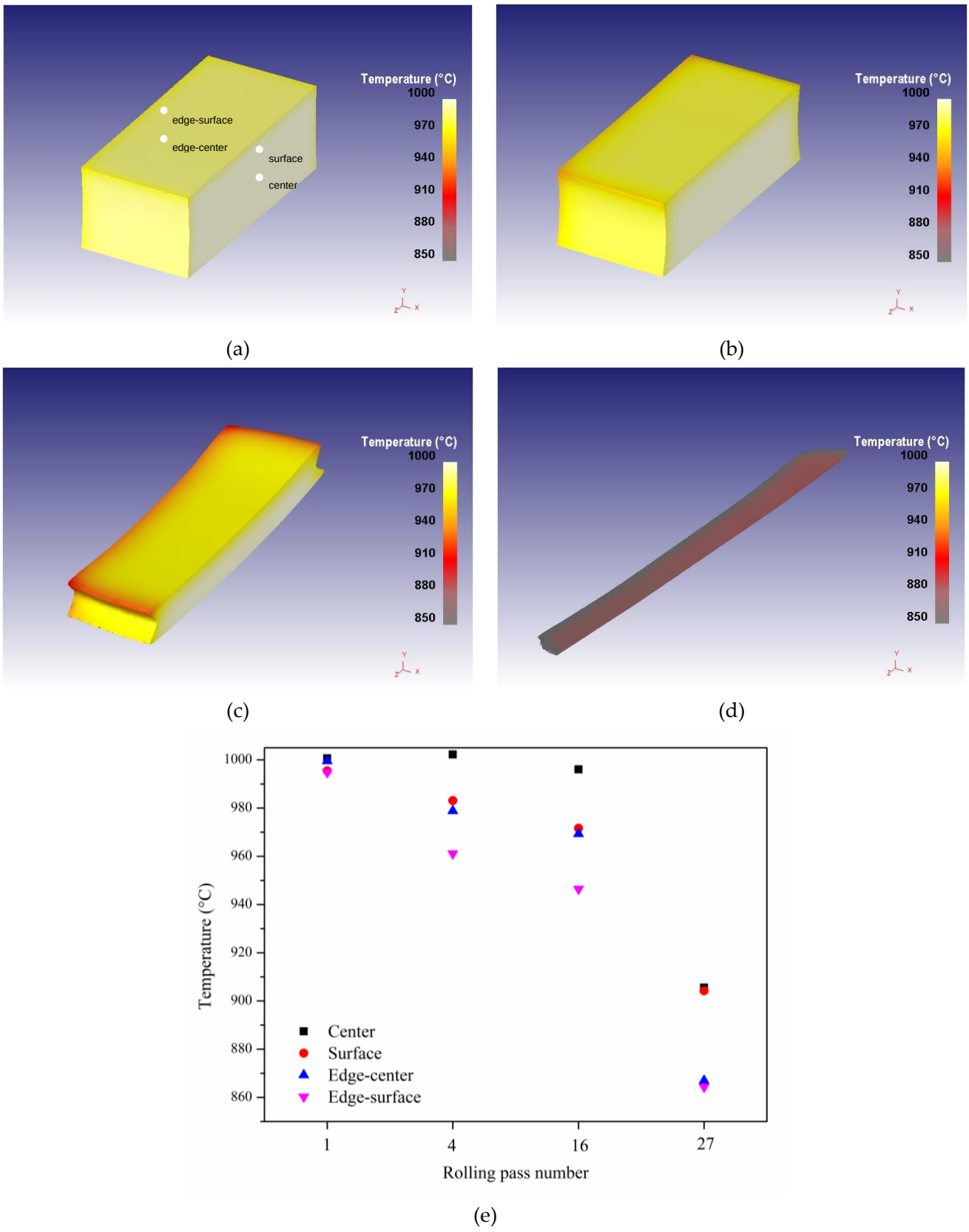

Figure 2. Temperature distribution for different rolling pass numbers: (**a**) pass #1, (**b**) pass #4, (**c**) pass #16 and (**d**) pass #27; (**e**) graph of the simulated temperature values evaluated in four points in the sheet.

The temperature distribution shows that in rolling pass # 1 the temperature is practically equal at the four points evaluated with a temperature close to 995 °C. As the number of rolling passes increases, the temperature decreases more in the edge-surface, edge-center and surface than in the center of the slab due to the heat transfer by the contact with the roller and convection heat transfer with the environment. The greatest loss of temperature occurs at the surface-edge of the slab reaching a temperature of 960 °C (rolling pass #4) and 946 °C (rolling pass #16), because in this area the morphology of the slab becomes thinner experiencing a higher heat transfer. The edge-center and surface point present a similar temperature, and the highest value is in the center of the slab because in this point there is not direct heat transfer to the environment. The last rolling pass #27 presents the lowest temperature of the whole process being 860 °C at the points evaluated at the edge of the sheet.

As it is exposed in the graph of Figure 2e, as the number of passes increases, the temperature decreases more on the edge-surface than in other points while the maximum temperature is in the center. The temperature gradient in the first rolling pass is negligible, but in the subsequent rolling passes a gradient of around 40 °C is observable, that is associated with the shape that the slab develops. In the last rolling pass, the temperatures in the center and surface are almost equal because the distance between the center and the surface has been reduced, generating that the temperature would be more homogeneous along the thickness.

Performing the simulation of the temperature distribution during each rolling cycle provided an excellent reference to determine the number of rolling passes that can be carried out experimentally without the temperature being below 850 °C, preventing the formation of ferrite, which in turn can cause workability problems during rolling.

3.1.2. Effective Strain Distribution

The effective strain is based on the following equation [21]:

$$\overline{\epsilon} = \frac{\sqrt{2}}{3}\sqrt{(\epsilon_1 - \epsilon_2)^2 + (\epsilon_2 - \epsilon_3)^2 + (\epsilon_3 - \epsilon_1)^2} \quad (1)$$

where, $\epsilon_1, \epsilon_2 \; y \; \epsilon_3$ are the principal strain in each axis and $\overline{\epsilon}$ is the effective strain.

In Figure 3a–d, the results obtained for the simulation of rolling passes #1, #4, #16 and #27 are presented. From these results, it can be observed that the effective strain is greater on the surface than in the center at each rolling pass, due to the direct contact between sheet surface and rollers. It should be noted that the strain increases between each rolling pass during the same cycle, since the strain is partially accumulated. However, at the start of each rolling cycle a reheating step is performed and, in that case, it is considered that the strain of the slab is eliminated by means of the softening processes that the material can experience.

According to the simulation results, the effective strain increases with the rolling passes for the evaluated points. As seen in Figure 2e, the maximum value is present in the surface point reaching a value up to 0.92 mm/mm. Another aspect that stands out in the simulation is that, as the number of rolling passes increases, the difference between the effective strain in the surface and the center becomes greatest by around 0.1, 0.35 and 0.36 for the rolling passes #1, #4 and #16, but the last pass presents a minimum difference of 0.07. This is due to the distance being smaller between the two rollers and therefore, the strain generated by the rollers on both surfaces is closer to the central zone, so the strain gradients are lower and the strain begins to be mostly homogeneous.

Simulation of the strain distribution in the sheet can help to identify possible zones of localized plastic flow and to display if the flow is predominantly uniform or heterogeneous. In addition, knowing the strain experienced by the sheet in local points permits to evaluate questions related to phase transformations that the material may undergo during the hot rolling process [6].

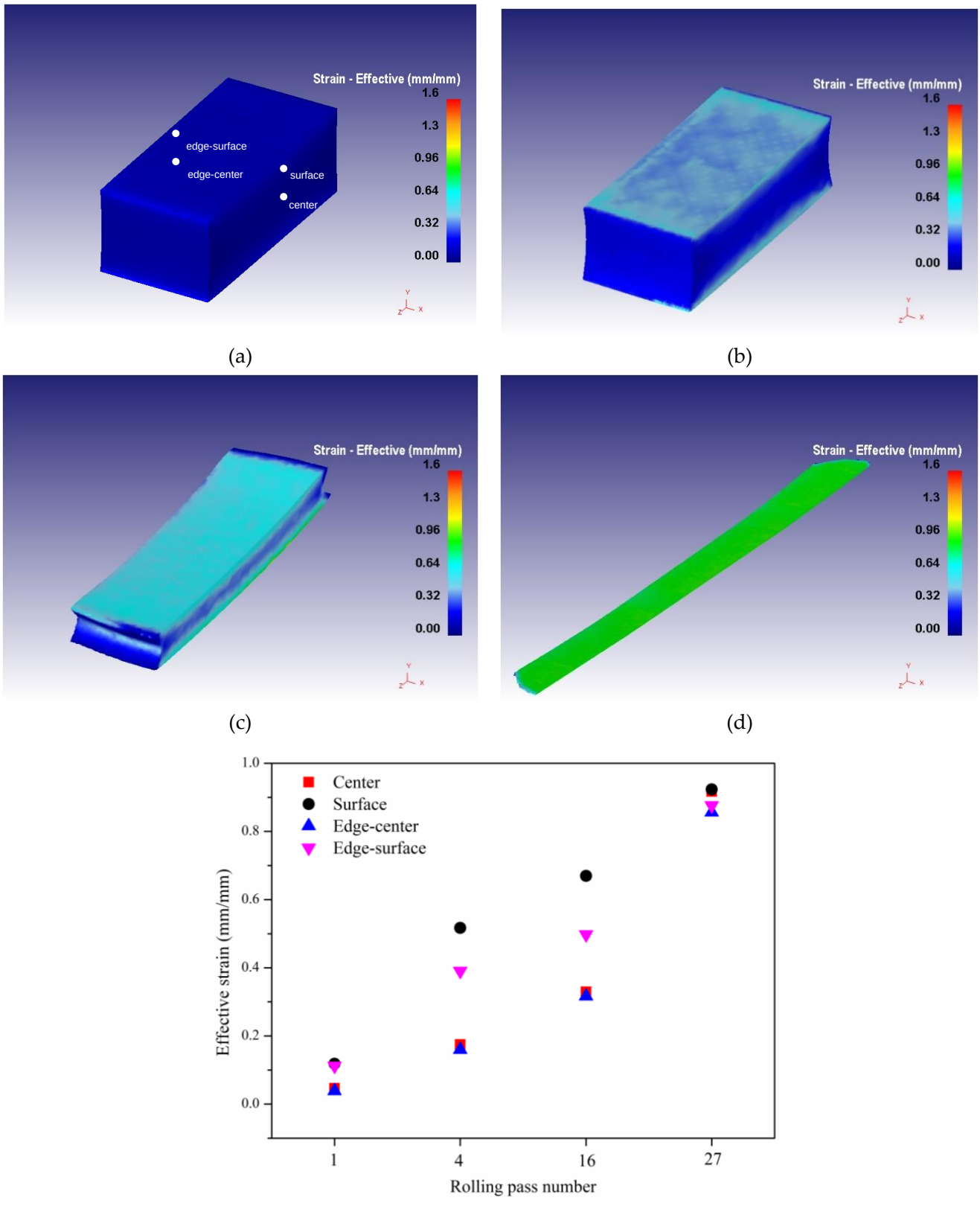

Figure 3. Effective strain distribution for different rolling pass numbers: (**a**) pass #1, (**b**) pass #4, (**c**) pass #16 and (**d**) pass #27; (**e**) graph of the simulated effective strain values evaluated in four points in the sheet.

3.1.3. Damage Factor

Damage generally relates to the likelihood of fracture in a slab, which occurs when the damage factor C reaches a critical value C* [22]. After the hot rolling process, edge cracking is often found on the lateral parts of the slab. In this sense, it is possible to obtain information about the fracture occurrence during hot rolling with the damage factor obtained by FEM simulations, and this factor can be used to predict crack creation in forming operations.

The normalized Cockcroft–Latham criterion [23] was selected to evaluate this damage factor, which is calculated by DEFORM-3D according to the following expression:

$$C = \int^{\varepsilon_f} \frac{\sigma^*}{\sigma}\, d\bar{\varepsilon} \tag{2}$$

where σ^*, σ, $\bar{\varepsilon}$ and ε_f denote the maximum component of tensile stress, the effective stress, the effective strain and the fracture strain, respectively. The normalized Cockcroft–Latham criterion during metalworking has been associated with fracture strain (ε_f) measured from uniaxial tension tests [22,24], which correspond to the C* value. In this work, a C* value of 0.37 was selected according to the hot tensile test results for a similar steel presented by Wang et al. [25].

Typical distributions of FEM predictions for damage factor C during the hot rolling process at rolling passes #1, #4, #16 and #27 are shown in Figure 4a–d. The damage factor values for the evaluated points are presented in Figure 4e. The damage had the lowest values at the center and surface of the slab. The greatest values were found on the side edges, especially on the edge-surface, the achieved values at this point were 0.035, 0.115, 0.187 and 0.435 for rolling passes #1, #4, #16 and #27, respectively. A gradual increment is noticed due to the concave shape that the slab exhibited in the side edges. It is important to remark that the obtained values were less than the C* value of 0.37, except for the last pass which means that the last pass should be carried out with caution. To decrease the damage on these edges, it is recommended to modify the initial morphology of the slab by machining a certain curvature on the edges, which has been suggested before by Dieter et al. [26]; however, this implies more mechanical processing on the slab and therefore a higher cost.

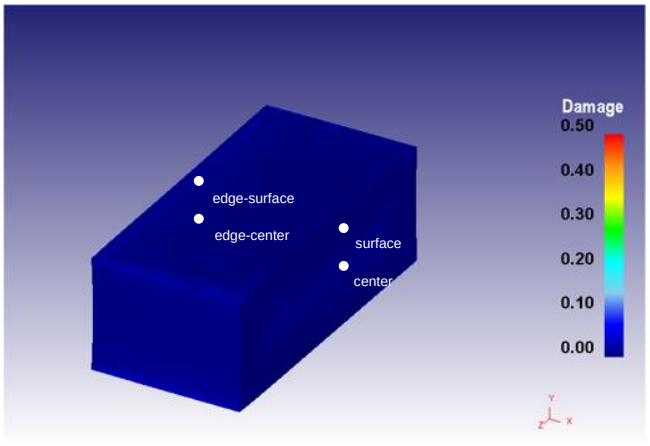

(a)

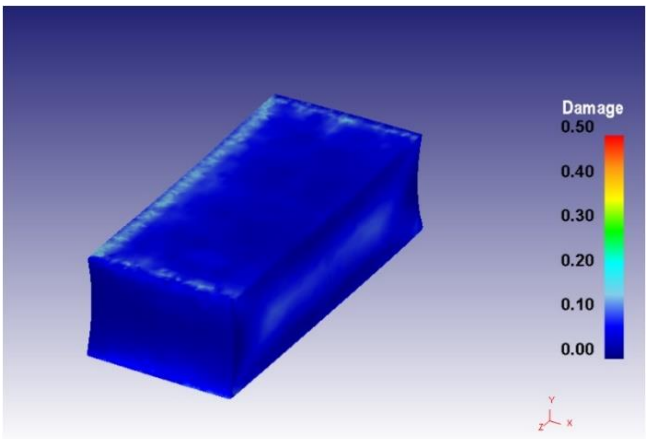

(b)

Figure 4. *Cont.*

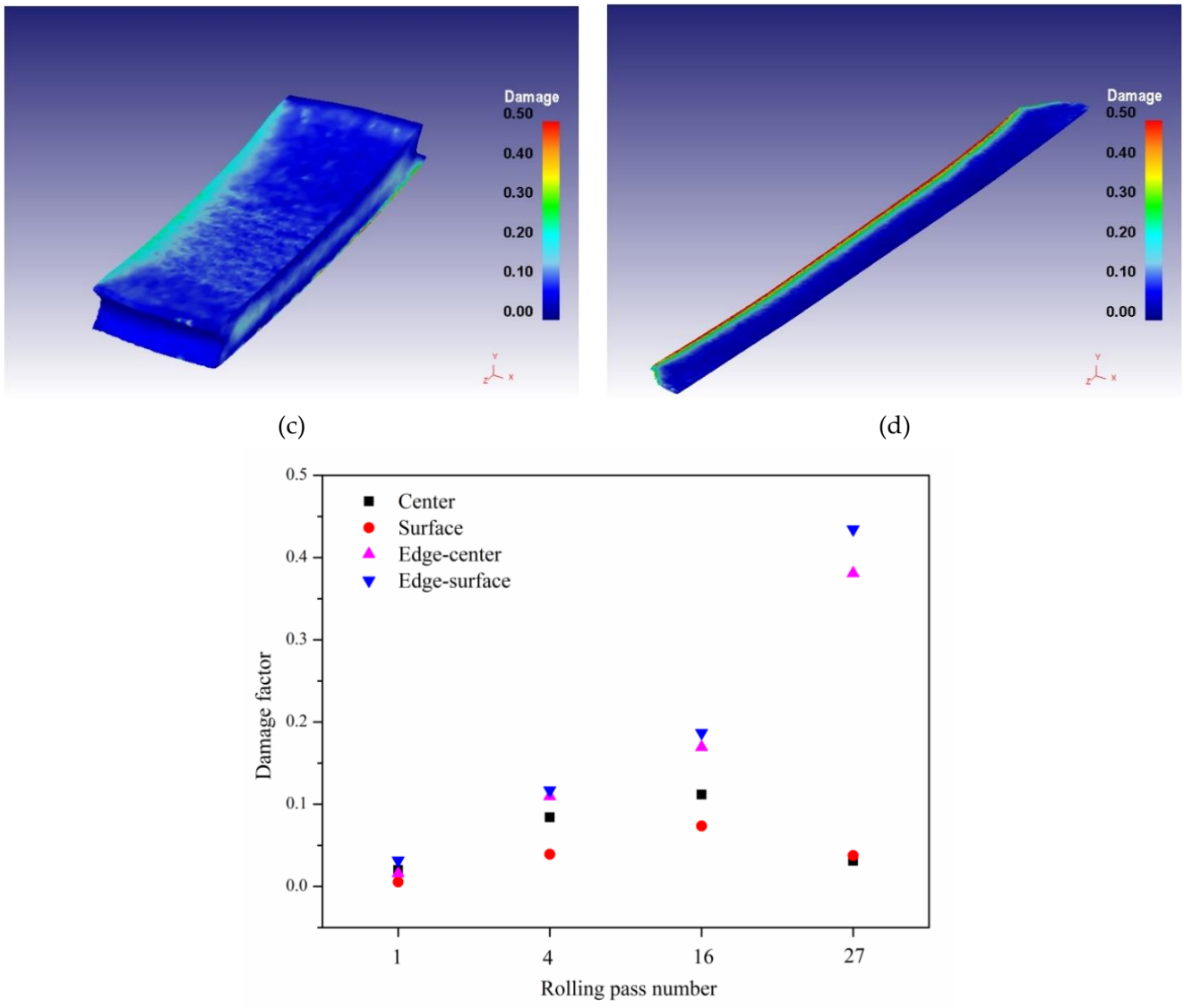

Figure 4. Damage factor values for different rolling pass numbers: (**a**) pass #1, (**b**) pass #4, (**c**) pass #16 and (**d**) pass #27; (**e**) graph of the simulated damage factor values evaluated in four points in the sheet.

Finally, a summary of the obtained values for the different analyzed rolling parameters is presented in Table 3. The displayed values correspond to an average of the four evaluated points (center, surface, edge-center and edge-surface). The temperature shows a decrease as more rolling passes are applied because of the heat transfer with the rollers and changes in the dimensions of the slab; the effective strain is bigger as the rolling passes increase since the distance between the rollers is getting smaller and the strain becomes more homogeneous; the effective strain rate is directly associated to the effective strain, so it also presents an increment in their values; at last, the damage factor also increases but only on the edges of the slab, a fact that is correlated to the changes in the morphology of the zones.

Table 3. Process parameters obtained during the simulation of the hot rolling process of a medium Mn steel.

Rolling Pass Number	Mean Temperature (°C)	Average Effective ε (mm/mm)	Average Effective $\dot{\varepsilon}$ (s^{-1})	Average Damage Factor
1	998	0.079	0.828	0.018
4	981	0.311	0.937	0.087
16	971	0.453	1.757	0.135
27	885	0.893	4.212	0.221

3.2. Characterization of the Resultant Microstructure of the Hot Rolled Medium Mn Steel

The simulated results allowed to establish some of the parameters required for the experimental hot rolling process, especially the selection of the number of rolling passes between each step of reheating for avoiding a temperature drop below 850 °C; in addition, the evaluation of the damage factor allowed to define the more susceptible areas for cracking in the sheet as well as the pass on which it could occur. As can be seen in Figure 5, the morphology of the sheet obtained experimentally is very similar to the simulated one. The side edges show a concave shape as the simulated results and more importantly, the presence of edge cracking was not observed in the experimental sample even though the damage factor was the highest in that zone.

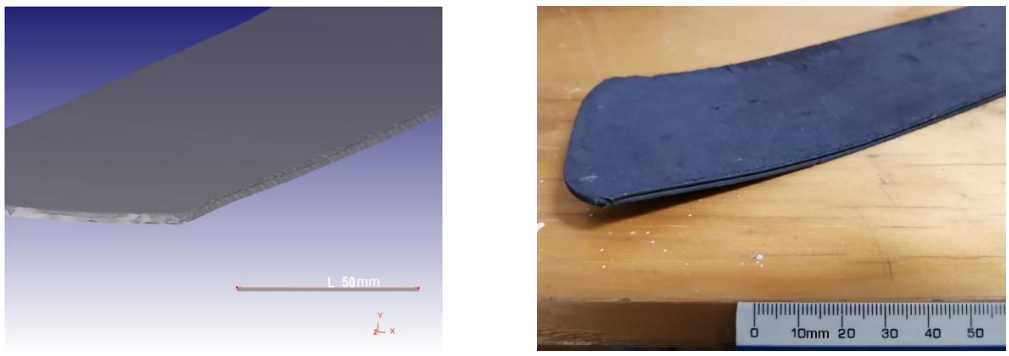

(a) (b)

Figure 5. Comparison between (**a**) the simulated and (**b**) experimental geometry of sheet.

The results of XRD of the sheet are shown in Figure 6. It can be noted that there are several strong peaks from austenite and some peaks that can be associated with α-ferrite and/or α′-martensite phases. The XRD technique does not allow to differentiate the α-ferrite and α′-martensite phases since the low C content generates that the α′-martensite phase loss their tetragonality and presents body centered-cubic (bcc) crystalline structure like the α-ferrite. The MAUD software, which is based on the Rietveld refining method [27], was employed to perform a quantitative analysis. The obtained results exhibited 56 and 44 wt.% of the austenite and α-ferrite/α′-martensite phases (sigma = 1.24, R_{wp} (%) = 7.15).

It is important to mention that despite carrying out the rolling process at high temperature, it is possible to observe the presence of α′-martensite since the partition of C and Mn towards austenite does not occur completely, so part of the austenite is transformed into martensite when cooling to room temperature [28].

Figure 7 presents the OM micrographs of the medium Mn steel. In Figure 7a,b, a banded microstructure formed during the hot rolling process is observed and two phases are distinguished: one in a light gray color that is associated with α′-martensite and the other in a dark gray color that is related to austenite. Evidence of α-ferrite was not detected. The SEM micrographs show that the martensite has a lath type morphology, as can be seen in Figure 7c. Microhardness tests were employed for phase identification in those regions, the α′-martensite zones exhibited the greatest microhardness values of around 400 HV and the austenite zones corresponded to the softest phase with a value of around 310 HV; it is possible that α′-martensite microhardness values have certain influence of both phases

because between the martensite laths could exist thin layers of austenite that cannot be resolved by optical and scanning electron microscopy, a similar behavior of the hardness was found by Li et al. [29].

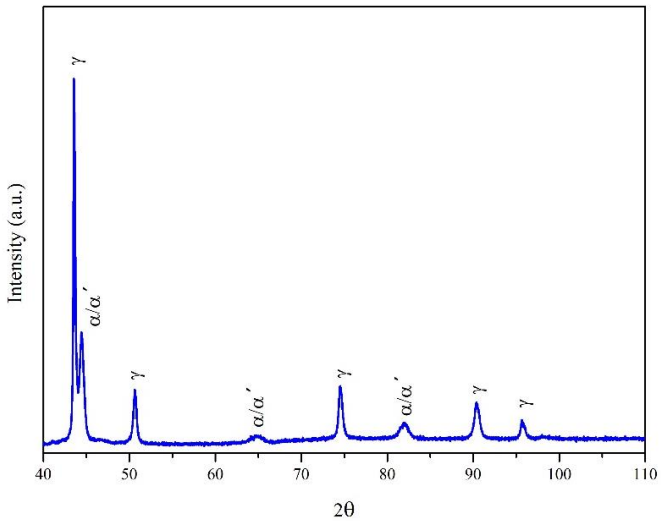

Figure 6. X-ray diffraction pattern of the hot rolled medium Mn steel.

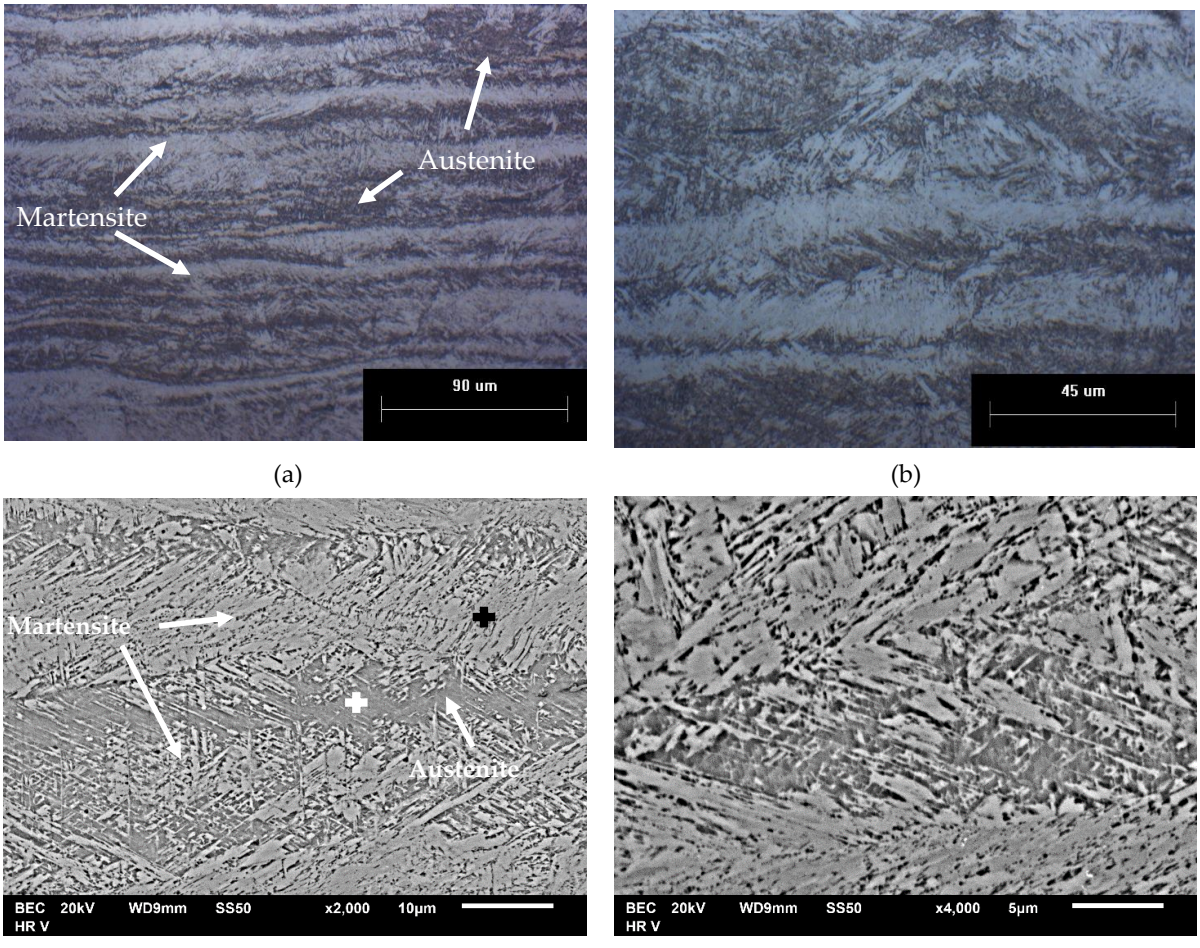

Figure 7. *Cont.*

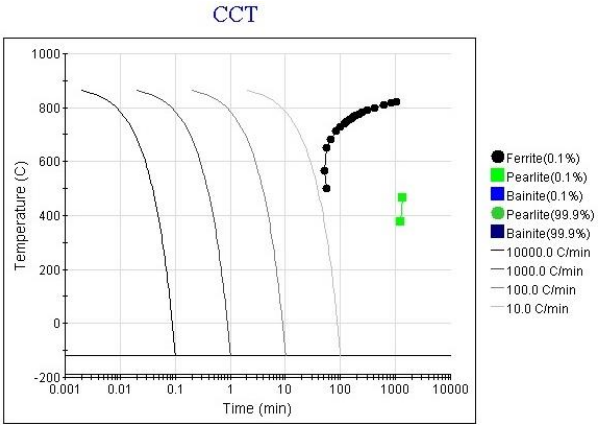

Element	C	Al	Si	Mn	Fe
Weight%	0.12	1.7	2.7	11	Bal.

(e)

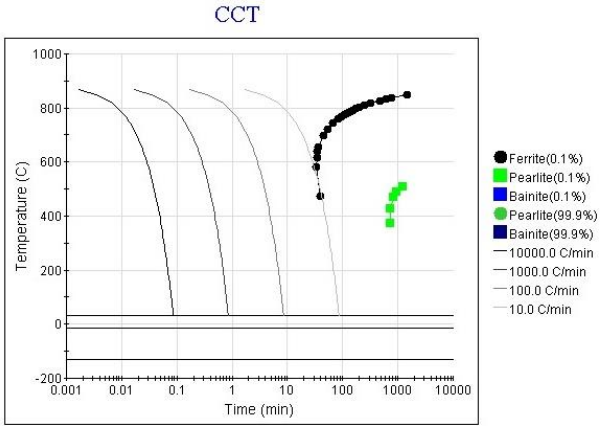

Element	C	Al	Si	Mn	Fe
Weight%	0.12	1.7	1.5	9	Bal.

(f)

Figure 7. Optical (**a**,**b**) and scanning electron microscope (**c**,**d**) images show the microstructure of the hot rolled medium Mn steel; EDX quantification in the austenite zone is indicated with a white cross in incise (**c**) and its respective CCT diagram is shown in (**e**); EDX quantification in the α'-martensite zone is indicated with a black cross in incise (**c**) and the respective CCT diagram is shown in (**f**).

In order to corroborate the phase identification, an energy-dispersive X-ray (EDX) analysis was realized to the austenite and α'-martensite zones. The average element quantification is presented in Figure 7e,f. As can be seen in the austenite zones (Figure 7e), the Mn content was higher than in the α'-martensite zones (Figure 7f) which agrees with the phase identification because to stabilize the austenite phase at room temperature a major content of Mn is required. The Continuous Cooling Transformation (CCT) diagrams simulated by JMatPro® software considering the composition of the two aforementioned zones and for a temperature close to 885 °C (which is the final average temperature of the sheet during the last pass of the rolling process), are shown in Figure 7e,f. For the austenite phase (Figure 7e), the M_s temperature is too low for martensite transformation to take place, while in the α'-martensite phase (Figure 7f) the M_s temperature is above room temperature so the presence of α'-martensite is promoted. The formation of other phases different from austenite occurs at very long cooling times, near or less than 10°/min, so it is expected that the microstructure of the steel is composed mainly of austenite and α'-martensite.

3.3. Mechanical Behavior of the Hot Rolled Medium Mn Steel

The results of the tensile tests for the hot rolled sample are given in Figure 8, with an ultimate tensile strength of 1116 MPa and an elongation of 27%. The mechanical properties of AHSS are represented by the product of ultimate tensile strength and total elongation (UTS × TE). The studied medium Mn steel presents a value of 30,132 MPa%, therefore it can be classified into the third generation of AHSS, which has a UTS × TE product higher than 25,000 MPa% [4].

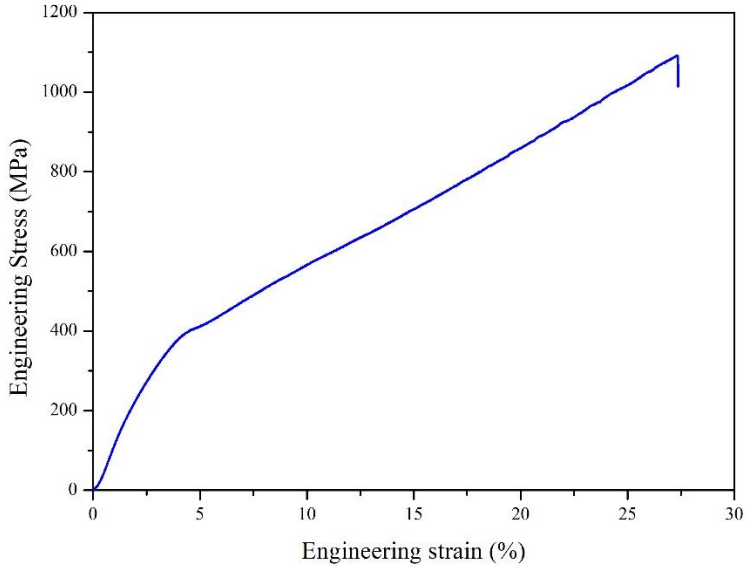

Figure 8. Engineering stress–strain curve of the hot rolled medium Mn steel.

The shape of the curve shows a fracture prior to the onset of necking at 1116 MPa. A maximum hardening is observed during plastic deformation [30], which is attributed to the formation of α'-martensite induced by deformation, also called Transformation Induced Plasticity (TRIP) effect. The continuous growing of martensite cores creates new interfaces that act as obstacles to the movement of dislocations [31]. After the tensile test, the sample was evaluated by XRD in an area close to fracture (Figure 9) and a decrease in the intensity of austenite peaks was clearly observed with respect to the hot rolled sample before the tensile test (Figure 6). The amount of austenite phase changed from 56 to 14 wt.% after the tensile test (sigma = 1.96, R_{wp} (%) = 9.30), which confirms the formation of α'-martensite and a little amount, 6 wt.%, of ε-martensite, both induced by deformation [32,33].

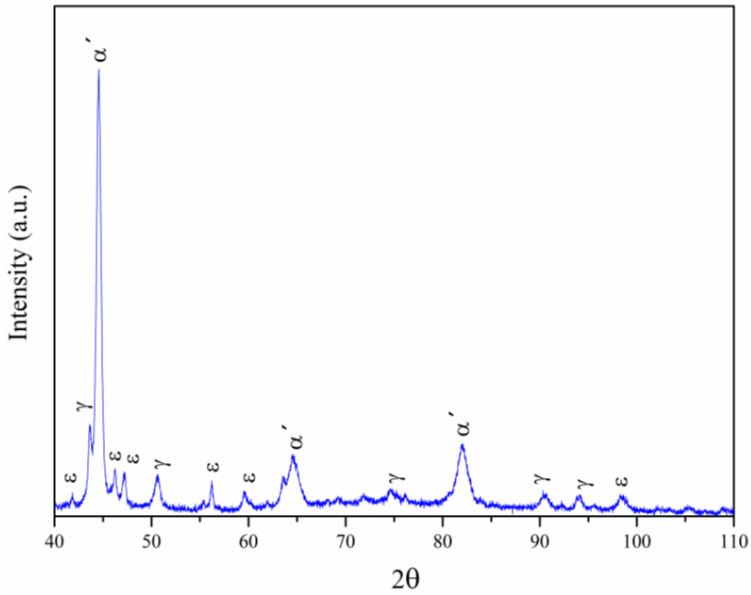

Figure 9. X-ray diffraction pattern after the tensile test of the hot rolled medium Mn steel.

4. Conclusions

(1) The computational simulation of the hot rolling process allowed to avoid the formation of detrimental phases and provide information of the zones with a higher probability of fracture according to changes in the temperature, effective strain and damage factor values for each rolling pass.

(2) The workability of the medium Mn steel observed during experimental hot rolling differs from the damage factor predictions in the sense that no fracture was detected after the last experimental rolling pass on which this parameter exhibited a value close to 0.43.

(3) A banded microstructure was observed in the hot rolled medium Mn steel, consisting of two different zones, one was related to austenite and the other to α'-martensite phases. This assumption was verified by an EDX analysis of these zones and their respective CCT diagram. In addition, ferrite phase formation was not predicted nor detected.

(4) A remarkable reduction of the austenite amount, from 56 to 14wt.%, after the tensile test of the hot rolled medium Mn steel evidenced the presence of the TRIP effect. The occurrence of this effect allowed to obtain a product of 30,132 MPa%, which permitted to catalogue this new steel in the third automotive generation.

Author Contributions: Conceptualization, A.C.G.-C. and J.L.H.-R.; methodology, P.G.-G. and J.L.H.-R.; software, J.L.H.-R.; validation, J.S.P.-C. and C.G.G.-R.; formal analysis, J.L.H.-R.; investigation, A.C.G.-C.; resources, M.O.R.-A. and J.d.J.C.-R.; writing—original draft preparation, A.C.G.-C.; writing—review and editing, J.L.H.-R.; visualization, J.L.H.-R.; supervision, J.L.H.-R.; project administration, P.G.-G. All authors have read and agreed to the published version of the manuscript.

Funding: This research received no external funding.

Institutional Review Board Statement: Not applicable.

Informed Consent Statement: Not applicable.

Data Availability Statement: The data presented in this study are available on request from the corresponding author. The data are not publicly available due to privacy reasons.

Acknowledgments: The authors gratefully appreciate the technical support given by Claudia Hernández, Alfredo Nuñez, Francisco Nuñez and Jesus Flores Sandoval from Instituto de Metalurgia-UASLP.

Conflicts of Interest: The authors declare no conflict of interest.

References

1. Zhao, J.; Jiang, Z. Thermomechanical processing of advanced high strength steels. *Prog. Mater. Sci.* **2018**, *94*, 174–242.
2. Benzing, J.T.; Poling, W.A.; Pierce, D.T.; Bentley, J.; Findley, K.O.; Raabe, D.; Wittig, J.E. Effects of strain rate on mechanical properties and deformation behavior of an austenitic Fe-25Mn-3Al-3Si TWIP-TRIP steel. *Mater. Sci. Eng. A* **2018**, *711*, 78–92. [CrossRef]
3. Grajcar, A.; Zalecki, W.; Burian, W.; Kozłowska, A. Phase equilibrium and austenite decomposition in advanced high-strength medium-Mn bainitic steels. *Metals* **2016**, *6*, 248. [CrossRef]
4. Nanda, T.; Singh, V.; Singh, V.; Chakraborty, A.; Sharma, S. Third generation of advanced high-strength steels: Processing routes and properties. *Proc. Inst. Mech. Eng. Part L J. Mater. Des. Appl.* **2019**, *233*, 209–238. [CrossRef]
5. Zhao, J.; Jiang, Z. (Eds.) *Rolling of Advanced High Strength Steels: Theory, Simulation and Practice*; CRC Press: Boca Raton, FL, USA, 2017; pp. 127–128.
6. Nakata, N.; Militzer, M. Modelling of microstructure evolution during hot rolling of a 780 MPa high strength steel. *ISIJ Int.* **2005**, *45*, 82–90. [CrossRef]
7. Tseng, A.A. A numerical heat transfer analysis of strip rolling. *J. Heat Trans.* **1984**, *106*, 512–517. [CrossRef]
8. Mazur, I.; Koinov, T. Quality control system for a hot-rolled metal surface. *J. Chem. Technol. Met.* **2014**, *49*, 71–76. [CrossRef]
9. Colas, R. Modelling heat transfer during hot rolling of steel strip. *Model. Simul. Mater. Sci. Eng.* **1995**, *3*, 437–453. [CrossRef]
10. Serajzadeh, S. Hot Rolling and Direct Cooling. In *Comprehensive Materials Processing*, 1st ed.; Van Tyne, C.J., Ed.; Elsevier: Oxford, UK, 2014; Volume 1, pp. 377–396.
11. Dwivedi, S.; Rana, R.S.; Rana, A.; Rajpurohit, S.; Purohit, R. Investigation of Damage in Small Deformation in Hot Rolling Process Using FEM. *Mater. Today Proc.* **2017**, *4*, 2360–2372. [CrossRef]
12. Obiko, J.O.; Mwema, F.M.; Bodunrin, M.O. Finite element simulation of $X_{20}CrMoV_{121}$ steel billet forging process using the Deform 3D software. *SN Appl. Sci.* **2019**, *1*, 1–10. [CrossRef]
13. Cavaliere, M.A.; Goldschmit, M.B.; Dvorkin, E.N. Finite element analysis of steel rolling processes. *Comput. Struct.* **2001**, *79*, 2075–2089. [CrossRef]
14. Rath, S. Computer simulation of hot rolling of flat products. *Softw. Eng.* **2016**, *4*, 75–81.
15. Huang, C.Q.; Deng, H.; Diao, J.P.; Hu, X.H. Numerical simulation of aluminum alloy hot rolling using DEFORM-3D. (2011, June). In *Proceedings of the 2011 IEEE International Conference on Computer Science and Automation Engineering, Shanghai, China, 10–12 June 2011*; IEEE: Piscataway, NJ, USA, 2011; Volume 3, pp. 378–381.

16. Kumar, A.; Rath, S.; Kumar, M. Simulation of plate rolling process using finite element method. *Mater. Today Proc.* **2020**, *42*, 650–659. [CrossRef]
17. Faini, F.; Attanasio, A.; Ceretti, E. Experimental and FE analysis of void closure in hot rolling of stainless steel. *J. Mater. Process. Technol.* **2018**, *259*, 235–242. [CrossRef]
18. Li, H.; Li, T.; Li, C.; Wang, Z.; Wang, G. Improvement of longitudinal performance uniformity of hot-rolled coils for cold-rolled DP980 steel. *Metals* **2020**, *10*, 382. [CrossRef]
19. Wang, H.; Yan, Y.; Jia, F.; Han, F. Investigations of fracture on DP980 steel sheet in roll forming process. *J. Manuf. Process* **2016**, *22*, 177–184. [CrossRef]
20. Vega, M.; Medina, S.; Chapa, M.; Quispe, A. Determination of Critical Temperatures (Tnr, Ar3, Ar1) in Hot Rolling of Structural Steels with Different Ti and N Contents. *ISIJ Int.* **1999**, *39*, 1304–1310. [CrossRef]
21. Deform-User Manual, S.F.T.C. *Deform V11.1*; Deform-User Manual, S.F.T.C.: Columbus, OH, USA, 2010.
22. Si, J.; Gao, F.; Han, P.; Zhang, J. Simulation on extrusion process of TiAl alloy. *Intermetallics* **2011**, *19*, 169–174. [CrossRef]
23. Oh, S.I.; Chen, C.C.; Kobayashi, S. Ductile fracture in axisymmetric extrusion and drawing— part II: Workability in extrusion and drawing. *J. Inst. Eng.* **1979**, *101*, 36–44.
24. Ning, F.; Jia, W.; Hou, J.; Chen, X.; Le, Q. Construction of edge cracks pre-criterion model based on hot rolling experiment and simulation of AZ31 magnesium alloy. *Mater. Res. Express.* **2018**, *5*, 056528. [CrossRef]
25. Wang, Y.J.; Zhao, S.; Song, R.B.; Hu, B. Hot ductility behavior of a Fe–0.3 C–9Mn–2Al medium Mn steel. *Int. J. Miner. Metall. Mater.* **2021**, *28*, 422–429. [CrossRef]
26. Dieter, G.E.; Kuhn, H.A.; Semiatin, S.L. *Handbook of Workability and Process Design*; American Society of Metals: Geauga County, OH, USA, 2003; pp. 236–237.
27. Young, R.A. *The Rietveld Method*; Oxford University Press: Oxford, UK, 1993; p. 298.
28. Mishra, G.; Chandan, A.K.; Kundu, S. Hot rolled and cold rolled medium manganese steel: Mechanical properties and microstructure. *Mater. Sci. Eng. A* **2017**, *701*, 319–327. [CrossRef]
29. Li, Z.C.; Zhang, X.T.; Mou, Y.J.; Misra, R.D.K.; He, L.F.; Li, H.P. The impact of intercritical annealing in conjunction with warm deformation process on microstructure, mechanical properties and TRIP effect in medium-Mn TRIP steels. *Mater. Sci. Eng. A* **2019**, *746*, 363–371. [CrossRef]
30. Field, D.M.; Van Aken, D.C. Dynamic strain aging phenomena and tensile response of medium-Mn TRIP steel. *Metall. Mater. Trans. A* **2018**, *49*, 1152–1166. [CrossRef]
31. Lee, S.; Estrin, Y.; De Cooman, B.C. Effect of the strain rate on the TRIP–TWIP transition in austenitic Fe-12 pct Mn-0.6 pct C TWIP steel. *Metall. Mater. Trans. A* **2014**, *45*, 717–730. [CrossRef]
32. Ma, Y.; Song, W.; Bleck, W. Investigation of the microstructure evolution in a Fe-17Mn-1.5 Al-0.3 C steel via in situ synchrotron X-ray diffraction during a tensile test. *Materials* **2017**, *10*, 1129.
33. Weiss, M.; Mester, K.; Taylor, A.; Stanford, N. A critical assessment of deformation twinning and epsilon martensite formation in austenitic alloys during complex forming operations. *Mater. Charact.* **2018**, *145*, 423–434. [CrossRef]